

Electronic Supplementary Information (ESI) for Energy & Environmental Science.
This journal is © The Royal Society of Chemistry 2022

Electronic Supplementary Information

Environmental and economic potential of decentralised electrocatalytic ammonia synthesis powered by solar energy

Sebastiano C. D'Angelo,^{†a} Antonio J. Martín,^{†a} Selene Cobo,^a Diego Freire Ordóñez,^b

Gonzalo Guillén-Gosálbez,^{*a} and Javier Pérez-Ramírez^{††*a}

^a *Institute for Chemical and Bioengineering, Department of Chemistry and Applied Biosciences, ETH Zürich, Vladimir-Prelog-Weg 1, 8093 Zürich, Switzerland*

^b *Centre for Process Systems Engineering, Imperial College of Science, Technology and Medicine, South Kensington Campus, Roderic Hill Building, London SW7 2BY, United Kingdom.*

Table of contents

S.1. Mathematical model	2
S.2. Further details on the alternative scenarios compared	10
S.3. Further details on the environmental analysis	12
S.4. Further details on the economic assessment	15
S.5. Extended analyses of additional scenarios	17

This document contains the electronic supplementary material of the main manuscript. Specifically, we elaborate on the mathematical modelling followed to estimate the cost and environmental and human health impacts of the various technologies, including the associated assumptions and simplifications. We also provide further details on the data used in the environmental and economic calculations and provide some additional results, including a sensitivity analysis considering the main uncertain parameters.

S.1 Mathematical model

In this section, we describe the equations of the proposed ammonia leaf (NH₃-leaf) model.

Energy requirements

The total energy required is obtained applying the following equation:

$$\hat{E}_{\text{tot}} = \frac{E_{\text{required}}}{\dot{m}_{\text{NH}_3\text{prod}}} = \frac{E_{\text{electrolyser}}}{\dot{m}_{\text{NH}_3\text{prod}}} - \frac{E_{\text{FC}}}{\dot{m}_{\text{NH}_3\text{prod}}} + \frac{E_{\text{N}_2\text{sep}}}{\dot{m}_{\text{N}_2\text{feed}}} \cdot \frac{\dot{m}_{\text{N}_2\text{feed}}}{\dot{m}_{\text{NH}_3\text{prod}}} \quad (\text{Equation S1})$$

where:

- \hat{E}_{tot} is the total energy consumption of the system per unit of mass;
- E_{required} is the yearly energy consumption of the system;
- $\dot{m}_{\text{NH}_3\text{prod}}$ is the yearly mass production of ammonia;
- $E_{\text{electrolyser}}$ is the yearly energy consumption of the electrolyser;
- E_{FC} is the yearly energy production of the fuel cell;
- $E_{\text{N}_2\text{sep}}$ is the yearly energy consumption of the nitrogen PSA separation unit;
- $\dot{m}_{\text{N}_2\text{feed}}$ is the yearly nitrogen mass consumption.

The electrolyser's energy consumption is determined from the following relationship:

$$\hat{E}_{\text{electrolyser}} = \frac{E_{\text{electrolyser}}}{\dot{m}_{\text{NH}_3\text{prod}}} = \frac{\Delta\hat{H}_{\text{eN}_2\text{R}}}{\eta_{\text{ECE}}} \quad (\text{Equation S2})$$

where:

- $\hat{E}_{\text{electrolyser}}$ is the energy consumption of the electrolyser per unit of mass of ammonia;
- $\Delta\hat{H}_{\text{eN}_2\text{R}}$ is the enthalpy change associated with the overall reaction comprising the two half-reactions of nitrogen reduction to ammonia and water oxidation to oxygen per unit of mass of ammonia;
- η_{ECE} is the energy conversion efficiency (ECE), as defined in the main manuscript.

The energy produced by the fuel cell can be calculated through the following equation:

$$\begin{aligned}
\hat{E}_{FC} &= \frac{E_{FC}}{\dot{m}_{\text{NH}_3\text{prod}}} = && \text{(Equation S3)} \\
&= \frac{\dot{m}_{\text{H}_2} \cdot \text{LHV}_{\text{H}_2} \cdot \eta_{FC}}{\dot{m}_{\text{NH}_3\text{prod}}} = \\
&= \frac{E_{\text{electrolyser}} \cdot (1 - \eta_F) \cdot \eta_V \cdot \text{LHV}_{\text{H}_2} \cdot \eta_{FC}}{\Delta \hat{H}_{\text{eWS}} \cdot \dot{m}_{\text{NH}_3\text{prod}}} = \\
&= \frac{\hat{E}_{\text{electrolyser}} \cdot \dot{m}_{\text{NH}_3\text{prod}} \cdot (1 - \eta_F) \cdot \eta_V \cdot \text{LHV}_{\text{H}_2} \cdot \eta_{FC}}{\Delta \hat{H}_{\text{eWS}} \cdot \dot{m}_{\text{NH}_3\text{prod}}} = \\
&= \frac{\hat{E}_{\text{electrolyser}} \cdot \text{LHV}_{\text{H}_2} \cdot \eta_{FC} \cdot (1 - \eta_F) \cdot \eta_V}{\Delta \hat{H}_{\text{eWS}}}
\end{aligned}$$

where:

- \dot{m}_{H_2} is the yearly mass production of hydrogen;
- LHV_{H_2} is the lower heating value of hydrogen;
- η_{FC} is the fuel cell efficiency with respect to the lower heating value of hydrogen;
- η_F is the Faradaic efficiency of the NH_3 -leaf with respect to ammonia, as defined in the main manuscript;
- η_V is the energy-to-chemicals (or voltage) efficiency of the NH_3 -leaf, as defined in the main manuscript;
- $\Delta \hat{H}_{\text{eWS}}$ is the enthalpy change associated with the water splitting reaction per unit of mass of hydrogen.

Environmental analysis

The total environmental impact (see **Table S3** for further details on the exact entries taken from ecoinvent) was calculated with the following equation:

$$\begin{aligned}
\hat{I}_{\text{tot}}^i &= \sum_{e \in E} CF^{i,e} \cdot (\hat{E}_{\text{tot}} \cdot \text{LCI}_{\text{PV}}^e + \hat{E}_{\text{electrolyser}} \cdot \text{LCI}_{\text{electr constr.}}^e + && \text{(Equation S4)} \\
&+ \hat{E}_{FC} \cdot \text{LCI}_{FC \text{ constr.}}^e + \hat{m}_{\text{H}_2\text{O input}} \cdot \text{LCI}_{\text{H}_2\text{O}}^e + \\
&+ \hat{m}_{\text{electrolyte purge}} \cdot \text{LCI}_{\text{electrolyte}}^e + \\
&+ \hat{E}_{\text{electrolyser}} \cdot \alpha_{\text{electrolyte make-up}} \cdot \text{LCI}_{\text{electrolyte}}^e + \\
&+ \hat{E}_{\text{electrolyser}} \cdot \alpha_{\text{H}_2\text{O make-up}} \cdot \text{LCI}_{\text{H}_2\text{O}}^e)
\end{aligned}$$

where:

- \hat{I}_{tot}^i is the total environmental impact per unit of mass of pure ammonia on impact category i ;
- $CF^{i,e}$ is the characterisation factor quantifying the impact of elementary flow e on impact category i ;
- LCI_{PV}^e represents elementary flow e associated with solar energy from photovoltaic (PV) panels per unit of energy produced, where the elementary flows are estimated based on the solar PV capacity factor according to **Equation S5**;

- $LCI_{\text{electr constr.}}^e$ represents elementary flow e associated with the electrolyser construction per unit of electrolyser energy input;
- $LCI_{\text{FC constr.}}^e$ is elementary flow e associated with the fuel cell construction per unit of fuel cell energy output;
- $\hat{m}_{\text{H}_2\text{O input}}$ is the total amount of tap water fed to the overall conversion system, excluding the water used as make-up;
- $LCI_{\text{H}_2\text{O}}^e$ represents elementary flow e associated with water consumption per mass unit of water;
- $\hat{m}_{\text{electrolyte purge}}$ is the electrolyte mass that is fed to the electrolyser to replace the amount of electrolyte that leaves with the product;
- $LCI_{\text{electrolyte}}^e$ represents elementary flow e associated with the electrolyte consumption per unit of mass of electrolyte;
- $\alpha_{\text{electrolyte make-up}}$ is the electrolyte mass consumption in the electrolyser per unit of electrolyser energy input: $\alpha_{\text{electrolyte make-up}} = \frac{\hat{m}_{\text{electrolyte make-up}}}{\hat{E}_{\text{electrolyser}}}$;
- $\alpha_{\text{H}_2\text{O make-up}}$ is the make-up water mass consumption in the electrolyser per unit of electrolyser energy input: $\alpha_{\text{H}_2\text{O make-up}} = \frac{\hat{m}_{\text{H}_2\text{O make-up}}}{\hat{E}_{\text{electrolyser}}}$.

The PV capacity factor was used to adjust to different locations the elementary flows linked to solar electricity, following the relationship below:

$$LCI_{\text{PV}, x}^e = LCI_{\text{PV}, \text{base case}}^e \cdot \frac{\text{cap. fact.}_{\text{base case}}}{\text{cap. fact.}_x} \quad (\text{Equation S5})$$

where:

- $LCI_{\text{PV}, x}^e$ represents elementary flow e associated with solar energy from PV panels per unit of energy produced at location x , characterised by a PV capacity factor cap. fact._x ;
- $LCI_{\text{PV}, \text{base case}}^e$ represents elementary flow e associated with solar energy from PV panels per unit of energy produced, assuming the global average PV capacity factor considered in ecoinvent, ($\text{cap. fact.}_{\text{base case}}$), *i.e.*, 10.98%.

In addition to this, the required water input was calculated through the following equations:

$$\hat{m}_{\text{H}_2\text{O input}} = \hat{m}_{\text{H}_2\text{O feed}} + \hat{m}_{\text{H}_2\text{O dil}} \quad (\text{Equation S6a})$$

$$\hat{m}_{\text{H}_2\text{O feed}} = \frac{1}{WEF} \cdot (\hat{m}_{\text{H}_2\text{O reac}} - \hat{m}_{\text{H}_2\text{O FC}}) \quad (\text{Equation S6b})$$

$$\hat{m}_{\text{H}_2\text{O FC}} = \frac{\dot{m}_{\text{H}_2}}{\dot{m}_{\text{NH}_3\text{prod}}} \cdot \frac{MM_{\text{H}_2\text{O}}}{MM_{\text{H}_2}} = \frac{\hat{E}_{\text{electrolyser}} \cdot (1 - \eta_F) \cdot \eta_V}{\Delta \hat{H}_{\text{eWS}}} \cdot \frac{MM_{\text{H}_2\text{O}}}{MM_{\text{H}_2}} \quad (\text{Equation S6c})$$

where:

- $\hat{m}_{\text{H}_2\text{O feed}}$ is the water entering the reverse osmosis unit to be converted into demineralised water, per unit of mass of ammonia;
- $\hat{m}_{\text{H}_2\text{O dil}}$ is the water needed downstream to dilute the product to the concentration required for fertigation, per unit of mass of ammonia. This amount also includes the small fraction of water that replaces what leaves the electrolyser in the product stream;

- WEF is the water efficiency factor, defined as the ratio between mass output and mass input associated with the reverse osmosis pre-treatment unit;
- $\hat{m}_{H_2O_{\text{reac}}}$ is the amount of demineralised water fed to the electrolyser unit, per unit of mass of ammonia;
- $\hat{m}_{H_2O_{\text{FC}}}$ is the amount of demineralised water produced by the fuel cell, per unit of mass of ammonia;
- MM_{H_2O} is the molar mass of water;
- MM_{H_2} is the molar mass of hydrogen.

Economic analysis

The economic performance of the NH_3 -leaf system was quantified through the levelised cost of ammonia (LCOA), which can be calculated as follows (see e.g. Sinnott and Towler¹):

$$LCOA = \frac{CAPEX_{\text{tot}} + OPEX_{\text{tot}}}{\dot{m}_{NH_3_{\text{prod}}} \cdot \sum_{t=1}^{t_{\text{lifespan}}} \frac{\alpha_{\text{prod. cap.}, t}}{(1 + DR)^t}} \quad (\text{Equation S7})$$

This value accounts for both the capital expenditures ($CAPEX_{\text{tot}}$) and the operating expenditures ($OPEX_{\text{tot}}$) of ammonia production throughout the lifespan (t_{lifespan}) of the project (30 years).

We estimated the LCOA considering a nominal ammonia production at steady-state ($\dot{m}_{NH_3_{\text{prod}}}$) of 100 kg per year of N-fertilier, i.e., the amount needed to fertilize one hectare of agricultural field (or, equivalently, 121 kg of ammonia per hectare per year).² $\alpha_{\text{prod. cap.}, t}$ is the fraction of nominal capacity assumed to be supported by the system each year of production (see also **Table S6**). Given the modularity of all the system components, we assume that the LCOA scales up linearly with the ammonia production capacity. The costs were discounted through the years assuming a constant discount rate (DR), here considered equal to 6.4% per year.³ The different contributions are outlined here in detail.

Capital expenditure

The capital expenditure can be approximated with the following equation:

$$CAPEX_{\text{tot}} = CAPEX_{\text{el.}} + CAPEX_{\text{FC}} + CAPEX_{\text{PV}} + \text{Cost}_{\text{decomm.}} \quad (\text{Equation S8})$$

where:

- $CAPEX_{\text{tot}}$ is the total capital expenditure during the overall lifetime of the system;
- $CAPEX_{\text{el.}}$ is the capital expenditure associated with the NH_3 -leaf electrolyser;
- $CAPEX_{\text{FC}}$ is the capital expenditure associated with the hydrogen fuel cell;
- $CAPEX_{\text{PV}}$ is the capital expenditure associated with the solar PV panels.
- $\text{Cost}_{\text{decomm.}}$ is the decommissioning cost at the end of the lifespan, included to produce conservative estimates.

The CAPEX of the NH_3 -leaf electrolyser was calculated as:

$$\text{CAPEX}_{\text{el.}} = \text{CAPEX}_{\text{el., in. inv.}} + \text{CAPEX}_{\text{el., st. repl.}} \quad (\text{Equation S9})$$

where:

- $\text{CAPEX}_{\text{el., in. inv.}}$ is the capital expenditure associated with the initial investment in the electrolyser;
- $\text{CAPEX}_{\text{el., st. repl.}}$ is the capital expenditure associated with the replacement of the active components of the electrolyser after their end-of-life.

The first of these contributions can be calculated as:

$$\text{CAPEX}_{\text{el., in. inv.}} = \hat{E}_{\text{electrolyser}} \cdot C_{\text{electrol.}} \cdot \dot{m}_{\text{NH}_{3\text{h. prod.}}} \cdot \sum_{t=-1}^{t_{\text{lifespan}}} \frac{\alpha_{\text{CAPEX el.,}t}}{(1 + \text{DR})^t} \quad (\text{Equation S10})$$

where:

- $C_{\text{electrol.}}$ is the purchase cost of the electrolyser, in $\text{USD}_{2020} \text{ kW}_{\text{input}}^{-1}$, assuming a similar cost per input electricity as a hydrogen electrolyser;
- $\dot{m}_{\text{NH}_{3\text{h. prod.}}} = \frac{\dot{m}_{\text{NH}_{3\text{prod}}}}{24 [\text{h d}^{-1}] \cdot 365 [\text{d a}^{-1}] \cdot \text{cap. fact.}_x}$ is the hourly ammonia production, accounting for the specific location with the PV capacity factor;
- $\alpha_{\text{CAPEX el.,}t}$ is the initial investment allocated to the electrolyser in year t ; here, the investment was split equally between the two years before the production begins;
- DR is the discount rate.

The cost associated with the replacement of the active components of the electrolyser is quantified with the following equation:

$$\begin{aligned} \text{CAPEX}_{\text{el., st. repl.}} &= \quad (\text{Equation S11}) \\ &= \hat{E}_{\text{electrolyser}} \cdot C_{\text{electrol.}} \cdot \dot{m}_{\text{NH}_{3\text{h. prod.}}} \cdot \alpha_{\text{el. st. repl.}} \cdot \sum_{t=1}^{\left\lfloor \frac{t_{\text{lifespan}}}{t_{\text{electrol.}}} \right\rfloor} \frac{1}{(1 + \text{DR})^{t_{\text{electrol.}} \cdot t}} \end{aligned}$$

where:

- $\alpha_{\text{el., st. repl.}}$ is the fraction of initial investment related to the replacement of active components of the electrolyser at their end-of-life;
- $t_{\text{electrol.}}$ is the lifespan of the active components of the electrolyser, in years.

The CAPEX of the hydrogen fuel cell was calculated using the following equation:

$$\text{CAPEX}_{\text{FC}} = \text{CAPEX}_{\text{FC, in. inv.}} + \text{CAPEX}_{\text{FC, st. repl.}} \quad (\text{Equation S12})$$

where the two contributors are homologous to those of the electrolyser CAPEX. The first of the two contributors can be summarised in the relationship below:

$$\text{CAPEX}_{\text{FC, in. inv.}} = \hat{E}_{\text{FC}} \cdot C_{\text{FC}} \cdot \dot{m}_{\text{NH}_{3\text{h. prod.}}} \cdot \sum_{t=-1}^{t_{\text{lifespan}}} \frac{\alpha_{\text{CAPEX FC,}t}}{(1 + \text{DR})^t} \quad (\text{Equation S13})$$

where:

- C_{FC} is the purchase cost of the fuel cell, in USD₂₀₂₀ kW_{output}⁻¹;
- $\alpha_{CAPEX_{FC,t}}$ is the initial investment allocated to the fuel cell in year t ; here the investment was allocated equally between the two years before production begins.

The cost associated with the replacement of the active components of the fuel cell are estimated with the following equation:

$$CAPEX_{FC, \text{st. repl.}} = \hat{E}_{FC} \cdot C_{FC} \cdot \dot{m}_{NH_3, \text{prod.}} \cdot \alpha_{FC, \text{st. repl.}} \cdot \sum_{t=1}^{\lfloor \frac{t_{\text{lifespan}}}{t_{FC}} \rfloor} \frac{1}{(1 + DR)^{t_{FC} \cdot t}} \quad (\text{Equation S14})$$

where:

- $\alpha_{FC, \text{st. repl.}}$ is the fraction of initial investment related to the replacement of active components of the fuel cell at their end-of-life;
- t_{FC} is the lifespan of the active components of the fuel cell, in years.

The CAPEX of the PV panels was calculated using the following equation:

$$CAPEX_{PV} = \frac{\hat{E}_{\text{tot}} \cdot \dot{m}_{NH_3, \text{prod.}} \cdot C_{PV} \cdot \frac{E_{\text{peak ref, PV, areal}}}{A_{\text{ref, PV}}} \cdot \sum_{t=1}^{t_{\text{lifespan}}} \frac{\alpha_{CAPEX_{PV,t}}}{(1 + DR)^t}}{SR_x \cdot 24 [\text{h d}^{-1}] \cdot 365 [\text{d a}^{-1}] \cdot 1 [\text{a}] \cdot \text{cap. fact.}_x \cdot \eta_{PV}} \quad (\text{Equation S15})$$

where:

- C_{PV} is the purchase cost of the PV panels, in USD₂₀₂₀ kWp⁻¹;
- The ratio $\frac{A_{\text{ref, PV}}}{E_{\text{peak ref, PV, areal}}}$, in m² kWp⁻¹, is taken from a reference plant in ecoinvent⁴ and is used to convert C_{PV} to a cost per unit of area, which still depends strictly only on the type of solar panels and not on the location;
- $\alpha_{CAPEX_{PV,t}}$ is the initial investment associated with the electrolyser in year t ; here, the investment was considered to be allocated equally between the two years before production begins;
- SR_x is the solar radiation, in kW m⁻², dependent on the location; here we used data from the literature to derive a polynomial linking the solar radiation with the PV capacity factor (see **Table S1**);
- η_{PV} is the solar-to-electricity efficiency of the solar panels.

Finally, the decommissioning cost was estimated through the following equation:

$$\text{Cost}_{\text{decomm.}} = \hat{E}_{\text{electrolyser}} \cdot C_{\text{electrol.}} \cdot \dot{m}_{NH_3, \text{prod.}} \cdot \alpha_{\text{decomm.}} \cdot \frac{1}{(1 + DR)^{t_{\text{lifespan}}}} \quad (\text{Equation S16})$$

where:

- $\alpha_{\text{decomm.}}$ is the fraction of CAPEX that corresponds to the decommissioning costs for the most expensive unit in the system, i.e., the electrolyser, assumed to represent the decommissioning expense of the system.¹

Replacement and decommissioning costs are considered as part of the CAPEX, since they are more intimately related to the purchase cost of the equipment.

Operating expenditure

The operating expenditures can be determined as follows:

$$\begin{aligned} \text{OPEX}_{\text{tot}} = & \text{OPEX}_{\text{O\&M, el.}} + \text{OPEX}_{\text{O\&M, FC}} + \text{OPEX}_{\text{O\&M, PV}} + \text{OPEX}_{\text{H}_2\text{O}} + \\ & + \text{OPEX}_{\text{electrolyte make-up}} \end{aligned} \quad (\text{Equation S17})$$

where:

- OPEX_{tot} is the total operating expenditure during the overall lifetime of the system;
- $\text{OPEX}_{\text{O\&M, el.}}$ represents the operation and maintenance costs of the electrolyser;
- $\text{OPEX}_{\text{O\&M, FC}}$ represents the operation and maintenance costs of the fuel cell;
- $\text{OPEX}_{\text{O\&M, PV}}$ represents the operation and maintenance costs of the PV panels;
- $\text{OPEX}_{\text{H}_2\text{O}}$ is the purchase cost of water for the reaction, downstream dilution, and make-up for the electrolyser;
- $\text{OPEX}_{\text{electrolyte make-up}}$ is the cost of the make-up electrolyte.

$\text{OPEX}_{\text{O\&M, el.}}$, $\text{OPEX}_{\text{O\&M, FC}}$ and $\text{OPEX}_{\text{O\&M, PV}}$ were quantified assuming that they are linear with respect to the purchase costs of the respective units.⁵⁻⁷ More precisely, the contribution associated with the operation and maintenance of the electrolyser is quantified as:

$$\text{OPEX}_{\text{O\&M, el.}} = \hat{E}_{\text{electrolyser}} \cdot C_{\text{electrol.}} \cdot \dot{m}_{\text{NH}_3, \text{prod.}} \cdot \alpha_{\text{O\&M, el.}} \cdot \sum_{t=1}^{t_{\text{lifespan}}} \frac{1}{(1 + \text{DR})^t} \quad (\text{Equation S18})$$

where:

- $\alpha_{\text{O\&M, el.}}$ is the fraction of CAPEX of the electrolyser corresponding to its annual operation and maintenance costs;
- DR is the discount rate.

Similarly, the homologous contribution for the fuel cell was defined with **Equation S19**:

$$\text{OPEX}_{\text{O\&M, FC}} = \hat{E}_{\text{FC}} \cdot C_{\text{FC}} \cdot \dot{m}_{\text{NH}_3, \text{prod.}} \cdot \alpha_{\text{O\&M, FC}} \cdot \sum_{t=1}^{t_{\text{lifespan}}} \frac{1}{(1 + \text{DR})^t} \quad (\text{Equation S19})$$

where $\alpha_{\text{O\&M, FC}}$ is defined analogously to $\alpha_{\text{O\&M, el.}}$.

¹ It would be possible to extend the decommissioning fraction to the overall system. However, since the contribution of this component currently lies in the range 0.18-0.35% of the total costs, with this assumption the decommissioning costs would remain below 1%.

In a similar fashion, the contribution from operation and maintenance associated with the PV panels are calculated as:

$$\text{OPEX}_{\text{O\&M, PV}} = \frac{\hat{E}_{\text{tot}} \cdot \dot{m}_{\text{NH}_3\text{prod}} \cdot C_{\text{PV}} \cdot \frac{E_{\text{peak ref, PV, areal}}}{A_{\text{ref, PV}}}}{SR_x \cdot 24 [\text{h d}^{-1}] \cdot 365 [\text{d a}^{-1}] \cdot 1 [\text{a}] \cdot \text{cap. fact.}_x \cdot \eta_{\text{PV}}} \cdot \alpha_{\text{O\&M, PV}} \cdot \sum_{t=1}^{t_{\text{lifespan}}} \frac{1}{(1 + \text{DR})^t} \quad (\text{Equation S20})$$

where $\alpha_{\text{O\&M, PV}}$ is defined analogously to $\alpha_{\text{O\&M, el.}}$ and $\alpha_{\text{O\&M, FC}}$.

The contribution of the water consumption to the OPEX can be split into three parts, two of them independent of the electrolyser efficiency and one, the make-up associated with the electrolyte solution, assumed to depend on the electrolyser efficiency:

$$\begin{aligned} \text{OPEX}_{\text{H}_2\text{O}} &= (\hat{m}_{\text{H}_2\text{O input}} + \hat{E}_{\text{electrolyser}} \cdot \alpha_{\text{H}_2\text{O make-up}}) \cdot \dot{m}_{\text{NH}_3\text{prod}} \cdot C_{\text{H}_2\text{O}} \cdot \sum_{t=1}^{t_{\text{lifespan}}} \frac{1}{(1 + \text{DR})^t} = (\text{Equation S21}) \\ &= (\hat{m}_{\text{H}_2\text{O feed}} + \hat{m}_{\text{H}_2\text{O dil}} + \hat{E}_{\text{electrolyser}} \cdot \alpha_{\text{H}_2\text{O make-up}}) \cdot \dot{m}_{\text{NH}_3\text{prod}} \cdot C_{\text{H}_2\text{O}} \cdot \\ &\quad \cdot \sum_{t=1}^{t_{\text{lifespan}}} \frac{1}{(1 + \text{DR})^t} \end{aligned}$$

where $C_{\text{H}_2\text{O}}$ is the cost of process water per kg.

Finally, the electrolyte contribution is calculated similarly to the make-up water:

$$\begin{aligned} \text{OPEX}_{\text{electrolyte make-up}} &= \\ &= (\hat{m}_{\text{electrolyte purge}} + \hat{E}_{\text{electrolyser}} \cdot \alpha_{\text{electrolyte make-up}}) \cdot \dot{m}_{\text{NH}_3\text{prod}} \cdot C_{\text{electrolyte}} \cdot \\ &\quad \cdot \sum_{t=1}^{t_{\text{lifespan}}} \frac{1}{(1 + \text{DR})^t} \end{aligned} \quad (\text{Equation S22})$$

where $C_{\text{electrolyte}}$ is the cost per kg of electrolyte.

The costs linked to the electrolyte solution make-up are often included in the operation and maintenance costs of the electrolyser.⁵ However, in this specific case, its contribution was considered potentially higher than in a standard hydrogen electrolyser and, thus, was estimated separately. This is because ammonia exits the system in the liquid phase, with a large part of the electrolyte solution, while in hydrogen electrolysers, hydrogen leaves the system in the gaseous phase with a negligible fraction of the electrolyte solution. In addition to this, we consider that the electrolyte make-up is inversely proportional to the selectivity of our system to ammonia, since a lower selectivity implies a bigger electrolyser, and the electrolyte make-up is assumed to increase linearly with the latter.

S.2 Further details on the alternative scenarios compared

The environmental impact and economic performance of the business-as-usual (BAU), blue Haber-Bosch (bHB), and green Haber-Bosch (gHB) were taken from a previous work.³ The system boundaries of these scenarios were expanded to encompass the addition of water and electrolyte to the produced ammonia, so that all the scenarios can produce functionally equivalent fertigation products. Thus, 45.33 L of water and $2.343 \cdot 10^{-2}$ kg of electrolyte (KHCO_3) are needed per kg of ammonia in these scenarios. It is relevant to highlight that this amount of water and potassium is much lower than the average amounts used for standard irrigation and fertilisation,^{8,9} implying that larger amounts of water and KHCO_3 would be needed to meet the crop demands.

Equation S5 was adopted to adjust the impact of electrolytic hydrogen production according to the location in the gHB scenario. The economic analysis of this scenario was adjusted accordingly, recalculating the LCOA by aligning the solar panels costs, the PV capacity factors, and the solar radiation with the values adopted in the NH_3 -leaf scenario. Moreover, the same optimistic assumption considered in the previous work about the replacement of active components in hydrogen electrolyzers was applied, in order to consider the much more advanced maturity level of this technology compared to the proposed NH_3 -leaf system. Specifically, we assumed that the gHB system could work in an ideal intermittency regime for a certain number of hours per year given by the capacity factor, and that the active components are substituted after the system reaches the end of life. Conversely, in the NH_3 -leaf scenario, the active components of the electrolyser and the fuel cell, are substituted after a fixed period, regardless of the actual active running time of the system, as shown in **Equations S11** and **S14**. Finally, **Table S1** reports the values of the PV capacity factors and the incident solar radiation associated with the average, best, and worst locations in the world. The reference year for the capacity factors is 2019, while for the solar radiation the year reported in the reference publication was considered. The grid of solar capacity factors was obtained using the Universal Transverse Mercator coordinate system,¹⁰ spacing each point 6° in longitude and 8° in latitude, from the parallel 72°N to the parallel 72°S . In addition to this, **Table S2** reports the composition of the 2019 power mix used to supply the electricity required by the Haber-Bosch (HB) process.

Table S1. PV capacity factors and solar radiation.

Parameter	Worst	Average	Best	Ref.
PV capacity factor [%]	5.60	10.98	26.26	4,11,12
Solar radiation [W m^{-2}]	93.75	166.67	281.25	13

Table S2. Composition of the global average power mix, adapted from the World Energy Outlook 2019.¹⁴ The name of the corresponding entries in ecoinvent is reported, except for bioenergy, which was modelled according to a previous work.³

Power source	ecoinvent entry	Share [%]
Coal	Electricity, high voltage {RoW} electricity production, hard coal APOS, S	38.11
Oil	Electricity, high voltage {RoW} electricity production, oil APOS, S	3.04
Natural gas	Electricity, high voltage {RoW} electricity production, natural gas, conventional power plant APOS, S	23.03
Nuclear	Electricity, high voltage {RoW} electricity production, nuclear, pressure water reactor APOS, S	10.23
Hydro	Electricity, high voltage {RoW} electricity production, hydro, run-of-river APOS, S	15.82
Bioenergy	See literature ³	2.39
Wind	Electricity, high voltage {RoW} electricity production, wind, 1-3MW turbine, onshore APOS, S	4.76
Geothermal	Electricity, high voltage {RoW} electricity production, deep geothermal APOS, S	0.34
Photovoltaic	Electricity, low voltage {RoW} electricity production, photovoltaic, 570kWp open ground installation, multi-Si APOS, S	2.23
Solar thermal	Electricity, high voltage {RoW} electricity production, solar thermal parabolic trough, 50 MW APOS, S	0.04

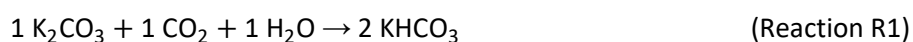
S.3 Further details on the environmental analysis

Table S3 compiles the inputs to the life cycle inventory of the NH₃-leaf system. Note that the values of the life cycle inventory, estimated with **Equations S1–S6c**, depend on the Faradaic efficiency and PV capacity factors.

Table S3. Inputs to the life cycle inventory of the NH₃-leaf and associated original references. The functional unit considered in the set of equations describing the NH₃-leaf system is indicated.

Input	Functional unit	Input name in reference	Ref.
Electricity from solar PVs	1 kWh	Electricity, low voltage {RoW} electricity production, photovoltaic, 570kWp open ground installation, multi-Si APOS, S	¹⁵
Electrolyser construction	1 kWh input	H ₂ (99.999 wt% purity) – Cell stack construction, alkaline water electrolysis ¹	³
Fuel cell construction	1 kWh output	Fuel cell stack ²	¹⁶
Electrolyte	1 kg	Potassium bicarbonate (KHCO ₃) {GLO} Table production, from potassium carbonate APOS, U	S4
Water	1 kg	Tap water {GLO} market group for APOS, S ³	¹⁵

The life cycle inventory of the electrolyte production is reported in **Table S4**. Because of the lack of data in ecoinvent and the literature, the production of this chemical was modelled consistently with the ecoinvent recommendations to fill data gaps,¹⁵ i.e., use of reagents in stoichiometric proportions in the feed and a 95% reaction yield. The industrial standard corresponds to the conversion from potassium bicarbonate.¹⁷ Since the reaction is exothermic, no energy input was considered. Finally, we report the exact names of the scenarios used to model the gHB, bHB and BAU in **Table S5**. Additional details on parameters used in the **Equations S1–S6c** are provided in **Table S6**.



¹ This entry, originally defined for a functional unit of 1 kg hydrogen produced, was rescaled with respect to the input electricity assuming 55 kWh input electricity per kg hydrogen produced; this result was then adjusted assuming conservatively the construction of 5 electrolysers to account for the maximum lifespan of 7 years for the active components.

² This entry, originally defined for 1 unit/kW, was rescaled assuming a 5-year lifespan and involving, consequently, the use of 6 fuel cells during the project lifetime.

³ Tap water was assumed as input for the electrolyser since a reverse osmosis unit is included in the system, consistently with what is included in a standard installation of PEM commercial electrolysers.

Table S4. Life cycle inventory inputs required to produce 1 kg of potassium bicarbonate.

Material	Amount [kg]
Potassium carbonate {GLO} market for APOS, U	0.726
Carbon dioxide, liquid {RoW} market for APOS, U	0.231
Tap water {GLO} market group for APOS, U	0.095

Table S5. Scenarios in ref.³ from which the pure ammonia life cycle inventories of the gHB, bHB, and BAU scenarios were taken.

Product	Scenario name in ref.³
Ammonia from green Haber-Bosch, 99.73 wt% purity	PEM-PV+2018mix
Ammonia from blue Haber-Bosch, 99.73 wt% purity	SMR+CCS _{SG+FG}
Ammonia from business-as-usual, 99.73 wt% purity	BAU

Table S6. Parameters and constants associated with **Equations S1–S6c.**

Parameter symbol	Parameter definition	Value	Unit	Ref.
$\Delta\hat{H}_{eN_2R}$	Specific enthalpy of reaction of nitrogen electroreduction to ammonia	20.43	MJ kg ⁻¹ NH ₃	18
$\Delta\hat{H}_{eWS}$	Specific enthalpy of reaction of water splitting into hydrogen and oxygen	141.79	MJ kg ⁻¹ H ₂	18
LHV_{H_2}	Lower heating value of hydrogen	120.03	MJ kg ⁻¹ H ₂	19
$\frac{E_{N_2 \text{ sep}}}{\dot{m}_{N_2 \text{ feed}}}$	Energy of separation of nitrogen from air	3.65×10^{-1}	kWh kg ⁻¹ N ₂	20
$\alpha_{\text{electrolyte make-up}}$	Amount of pure electrolyte make-up dependent on the electrolyser energy input	5.80×10^{-4}	kg K ₂ CO ₃ kWh ⁻¹ _{input}	21,22
$\alpha_{H_2O \text{ make-up}}$	Amount of water associated with electrolyte solution make-up dependent on the electrolyser energy input	5.78×10^{-2}	kg H ₂ O kWh ⁻¹ _{input}	21,22
WEF	Water efficiency factor for reverse osmosis unit.	47.06	%	23
η_V	Voltage efficiency	62.57	%	See main article
η_F	Faradaic efficiency	34.00–100.00	%	See main article
η_{ECE}	Energy conversion efficiency	21.27–62.57	%	See main article
η_{FC}	Fuel cell efficiency	60	%	24

S.4 Further details on the economic assessment

Table S7 reports the values of the parameters involved in the calculation of the LCOA.

Table S7. Relevant parameters and constants associated with **Equations S7–S22.**

Parameter symbol	Parameter definition	Value	Unit	Ref.
$C_{\text{electrol.}}$	Purchase cost of electrolyser unit	1197.11	USD ₂₀₂₀ kW ⁻¹ _{input}	25
$\alpha_{\text{CAPEX el.,}t}$	Allocation of initial investment in electrolyser to year t	$\begin{cases} 0.5 & \text{if } t=-1,0 \\ 0 & \text{else} \end{cases}$	-	3
DR	Discount rate	6.4	%	3
t_{lifespan}	Project lifetime ¹	30	a	7
$\alpha_{\text{prod. cap.,}t}$	Production capacity fraction with respect to full capacity in year t	$\begin{cases} 0.5 & \text{if } t=1 \\ 1 & \text{else} \end{cases}$	-	3
$\alpha_{\text{el., st. repl.}}$	Fraction of initial electrolyser CAPEX associated with the replacement cost of active components	15.00	%	25
$t_{\text{electrol.}}$	Lifetime of active components of the electrolyser ²	7	a	25
C_{FC}	Purchase cost of fuel cell unit	2943.71	USD ₂₀₂₀ kW ⁻¹ _{output}	6
$\alpha_{\text{CAPEX FC},t}$	Allocation of initial investment in fuel cell to year t	$\begin{cases} 0.5 & \text{if } t=-1,0 \\ 0 & \text{else} \end{cases}$	-	3
$\alpha_{\text{FC, st. repl.}}$	Fraction of initial fuel cell CAPEX associated with the replacement cost of active components	83.33	%	6
t_{FC}	Lifetime of active components of the fuel cell	5	A	6
C_{PV}	Purchase cost of solar panels	778.36	USD ₂₀₂₀ kWp ⁻¹	7
$A_{\text{ref, PV}}$	Reference area for installed PV modules	4273.50	m ²	4

¹ Coincident with the lifetime of the solar panels.

² Assumption estimated from average lifespan of commercial hydrogen electrolyzers.

Parameter symbol	Parameter definition	Value	Unit	Ref.
$E_{\text{peak ref, PV, areal}}$	Reference peak capacity for installed PV modules	570	kWp	4
$\alpha_{\text{CAPEX PV}, t}$	Allocation of initial investment in PV panels to year t	$\begin{cases} 0.5 & \text{if } t=-1,0 \\ 0 & \text{else} \end{cases}$	-	3
η_{PV}	Solar-to-power efficiency of PV panels	20	%	2
$\alpha_{\text{decomm.}}$	Fraction of initial electrolyser CAPEX associated with end-of-life decommissioning	10.00	%	25
$\alpha_{\text{O\&M, el.}}$	Fraction of initial electrolyser CAPEX that needs to be spent yearly to account for operation and maintenance of the unit	4.00	%	5
$\alpha_{\text{O\&M, FC}}$	Fraction of initial fuel cell CAPEX that needs to be spent yearly to account for operation and maintenance of the unit	4.00	%	6
$\alpha_{\text{O\&M, PV}}$	Fraction of initial PV panels CAPEX that needs to be spent yearly to account for operation and maintenance of the modules	2.00	%	7
$C_{\text{H}_2\text{O}}$	Cost of process water	5.20×10^{-5}	USD ₂₀₂₀ kg ⁻¹ H ₂ O	26
$C_{\text{electrolyte}}$	Cost of KHCO ₃ electrolyte	5.55	USD ₂₀₂₀ kg ⁻¹ KHCO ₃	26

S.5 Extended-analyses of additional scenarios

In this section, we show a sensitivity analysis of the results obtained for the NH₃-leaf scenario, performed by varying the voltage efficiency (**Fig. S1A**) and the units' costs (**Fig. S1B**). A sensitivity on the environmental impact of the electrolyser and fuel cell stack construction is provided in **Fig. S2**. Extended versions of **Fig. 3** and **Fig. 5**, where also the voltage efficiency was varied from 63 to 100% for the NH₃-leaf and the stack efficiency for the water electrolyser from 60 to 100% for the gHB scenario, are shown in **Fig. S3** and **Fig. S4**. Furthermore, **Fig. S5** and **Fig. S6** represent alternative versions of **Fig. 3** and **Fig. 5** where future aspirational values for the voltage efficiency of the NH₃-leaf and for the stack efficiency of water electrolyzers for the gHB scenario are considered. Moreover, the breakdown of the most important environmental metrics is reported in **Fig. S7**. **Fig. S8** and **Fig. S9** represent variations of **Fig. 3A** and **Fig. 5A**, respectively, that consider a configuration of the NH₃-leaf without fuel cell, assuming different fates for the hydrogen by-product. Finally, **Fig. S10** drafts a nitrate-producing system that expands the concept of NH₃-leaf for the far future.

As expected, the voltage efficiency (**Fig. S1A**) plays a very relevant role, especially for the carbon-related planetary boundaries and the carbon footprint, all varying in the range -24%/+119% with respect to the base case for voltage efficiencies of 80 and 30%, respectively. The impact on the other Earth-system processes shows a similar variation as in climate change, given the same underlying relationship, except for freshwater use. This is because the latter relies on additional parameters that are independent of the voltage efficiency, such as downstream dilution of the product, and thus lead to a narrower variation (-8%/+41%). Human health impacts vary similarly to the climate change impacts (-24%/+117%). In contrast to this, the LCOA shows a milder deviation (-18%/+88%) associated with the same change in voltage efficiency due to additional dependence on water dilution.

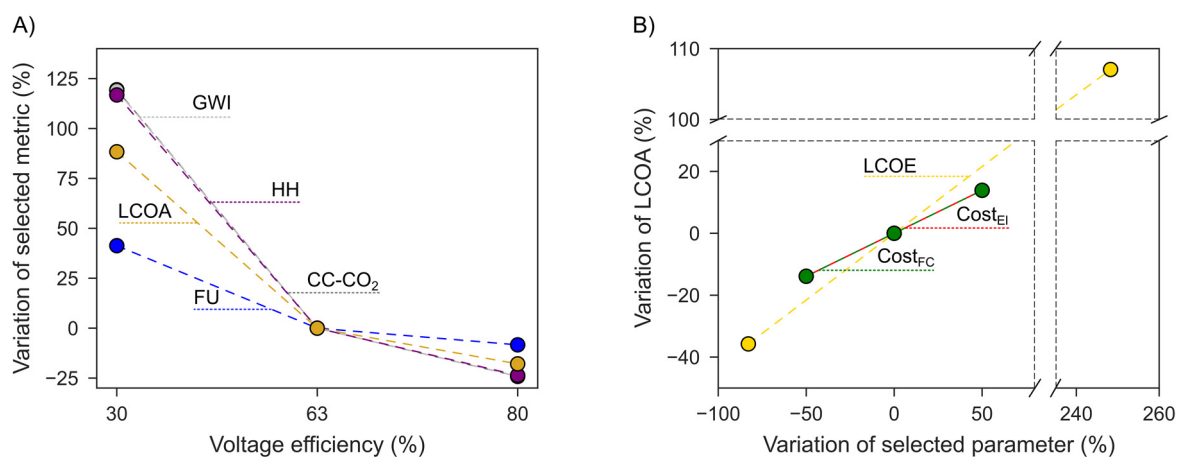


Fig. S1. (A–B) Sensitivity analysis of the results of the ammonia leaf (NH_3 -leaf) scenario, assuming a state-of-the-art Faradaic efficiency (34%) and global average PV capacity factor (11%). (A) Sensitivity analysis of the impacts on the climate change Earth-system process (CO_2 concentration as control variable, in dark grey), freshwater use (blue), global warming impacts (GWI, light grey), human health impacts (HH, purple), and levelised cost of ammonia (LCOA, gold) with respect to the voltage efficiency. (B) Sensitivity analysis of the LCOA, varying the levelised cost of electricity (LCOE, yellow), purchase cost of the electrolyser (Cost_{El} , red) and purchase cost of the fuel cell (Cost_{FC} , green). The LCOE was varied between 0.058 and 1.190 $\text{USD}_{2020} \text{ kWh}^{-1}$, moving from a realistic lower bound⁵⁰ up to the value of LCOE obtained for the worst location in the main article, assuming that only the LCOE contributes to the LCOA. These values correspond to a solar panel purchase cost in the range 224.7–1697.0 $\text{USD}_{2020} \text{ kWp}^{-1}$, considering the global average capacity factor. The purchase costs of the electrolyser and fuel cell were varied by $\pm 50\%$ relative to the value assumed for the base case.

In terms of economic impacts (**Fig. S1B**), the similar cost share of the electrolyser and fuel cell leads to a similar qualitative trend in the corresponding sensitivities. By varying the investment cost of the electrolyser and fuel cell by $\pm 50\%$ with respect to the base assumption, changes of $\pm 14\%$ can be observed for both cases in the final LCOA. A wider range was assumed for the LCOE, considering the lowest value projected in the literature and the worst-case estimation assumed in this study, i.e., the LCOE in the worst location.²⁷ With this approach, variations of $-83\%/+248\%$ lead to a $-36\%/+107\%$ change.

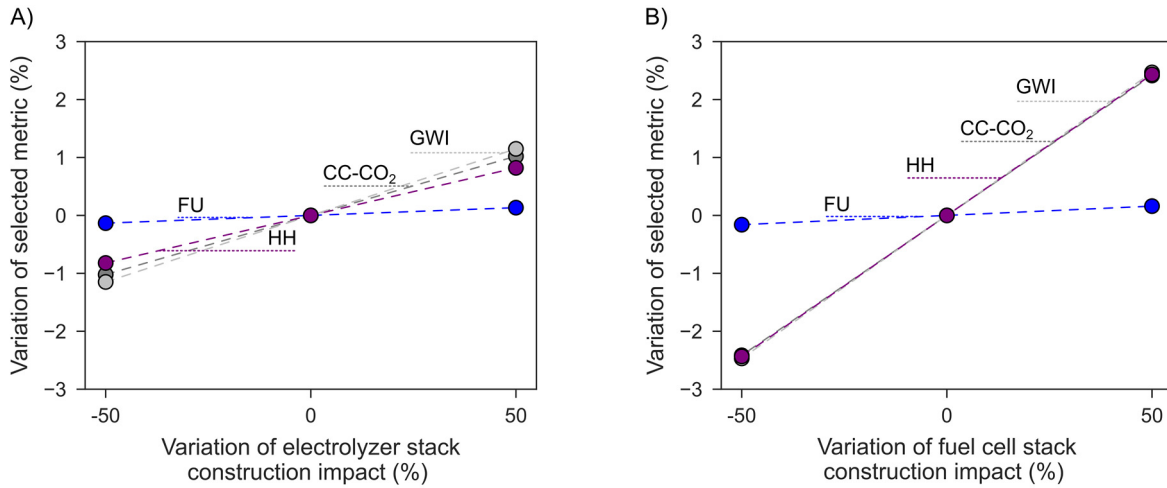


Fig. S2. Sensitivity analysis of the results of the ammonia leaf (NH_3 -leaf) scenario, assuming a state-of-the-art Faradaic efficiency (34%) and global average PV capacity factor (11%). The figure focuses on the impacts on the climate change Earth-system process (CO_2 concentration as control variable, CC- CO_2 , in dark grey), freshwater use (FU, blue), global warming impacts (GWI, light grey), and human health impacts (HH, purple) with respect to a variation of $\pm 50\%$ of the environmental impact of the electrolyser (A) and fuel cell stack (B) construction, relatively to the value assumed for the base case.

By observing the influence of the electrolyser and fuel cell stack construction on a selection of indicators (**Fig. S2**), it is evident that they play a minor role in the overall impact. Specifically, the sensitivity with respect to the electrolyser stack construction shows a variation of up to $\pm 1.1\%$ in the overall impact for all the considered indicators, while for the case of the fuel cell such variation increases up to $\pm 2.5\%$. The global warming impacts indicator is the most sensitive to changes in both electrolyser and fuel cell, within the selected indicators. Other indicators, such as freshwater use, show a negligible variation in the overall influence of these two units, with ranges within $\pm 0.2\%$ for both the sensitivity analyses. If other planetary boundaries are considered, the variation is very similar to the case of the climate change indicator, with the exception of stratospheric ozone depletion, that varies in the range $\pm 7\%$ and $\pm 5\%$ for a $\pm 50\%$ variation in the electrolyser and fuel cell stack construction impacts, respectively.

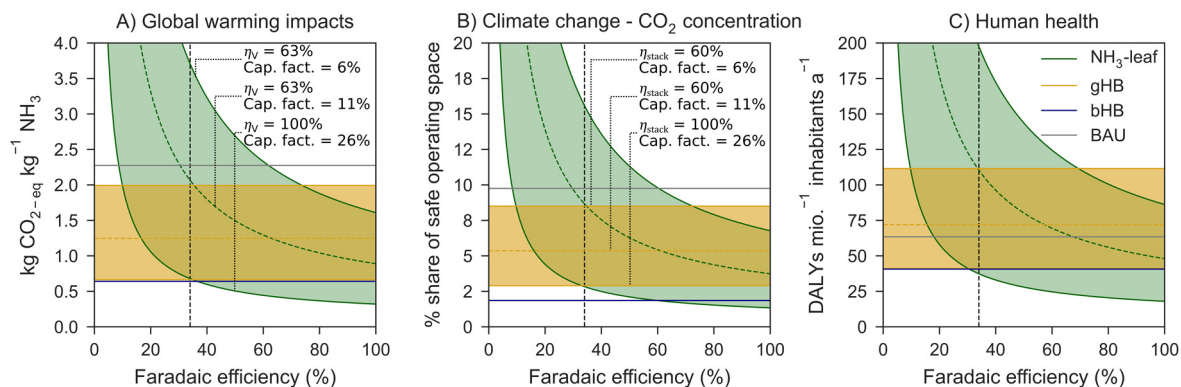


Fig. S3. (A–C) Sensitivities showing the environmental impacts of the ammonia leaf (NH_3 -leaf) on three selected metrics (A: global warming impacts; B: climate change – CO_2 concentration; C: human health) versus the Faradaic efficiency and comparison with the Haber-Bosch (HB) processes, namely, the green HB (gHB, yellow), blue HB (bHB, blue), and business-as-usual (BAU). The shaded green area represents the impact of the NH_3 -leaf varying, alongside the Faradaic efficiency, also the voltage efficiency in the range 63–100% and the capacity factor in the range 6–26%. The dashed green line represents the case assuming a voltage efficiency equal to 63% and the average capacity factor (11%). The shaded yellow area depicts the impact of the gHB case varying the stack efficiency in the range 60–100% and the capacity factor in the range 6–26%. The dashed yellow line represents the case assuming a stack efficiency of 60% and the average capacity factor (11%).

In line with what is shown in **Fig. S1**, the impact of an increase in voltage efficiency from an industrially viable value such as 63% up to an ideal case is much less relevant than the choice of the location and, thus, of the solar capacity factor (**Fig. S3**). The impact difference with varying voltage efficiencies increases with decreasing Faradaic efficiencies, given the same capacity factor. For example, the impact of global warming impacts (**Fig. S3A**) decreases by about 48% passing from an average to a high capacity factor while fixing the voltage efficiency at 63%; this difference increases to 67% if the voltage efficiency is also increased to 100%, alongside the capacity factor. At the same time, the differences obtained by fixing the Faradaic efficiency at 100% amount to 49% and 64%, respectively. Similar qualitative trends can be obtained for the other two impacts shown in **Fig. S3**, namely, climate change – CO_2 concentration (**Fig. S3B**) and human health (**Fig. S3C**). However, an increase to 100% voltage efficiency can lead, notably, to a shift of the breakeven Faradaic efficiency with respect to the bHB case to values below the current best state-of-the-art for the best location for human health (31%). For global warming impacts and climate change – CO_2 concentration a breakeven Faradaic efficiency of 37% and 60% with the bHB can be highlighted, respectively, showing a decrease of about 42% with respect to the same values for a 63% voltage efficiency.

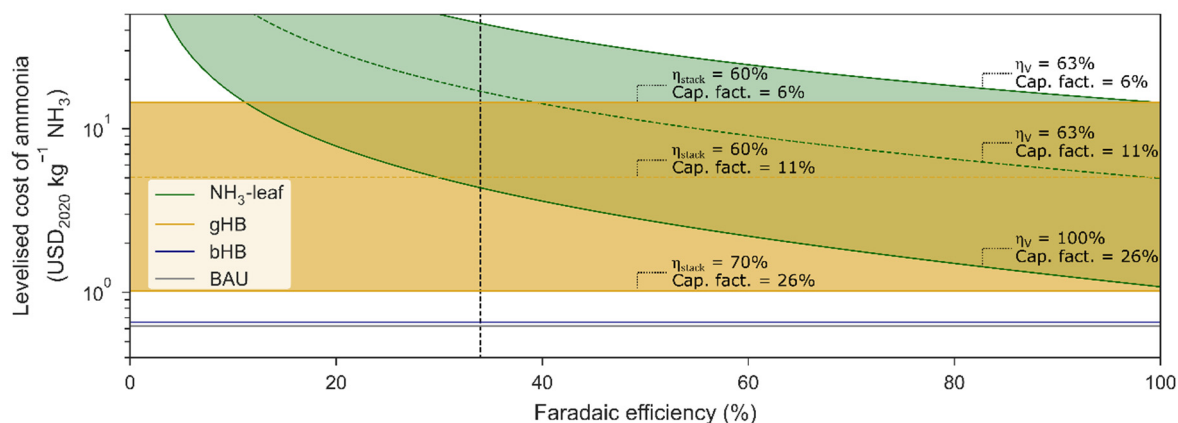


Fig. S4. Economic performance of the ammonia leaf (NH₃-leaf) versus the Faradaic efficiency and comparison with the Haber-Bosch (HB) processes, namely, the green HB (gHB, yellow), blue HB (bHB, blue), and business-as-usual (BAU). The shaded green area represents the impact of the NH₃-leaf varying, alongside the Faradaic efficiency, also the voltage efficiency in the range 63–100% and the capacity factor in the range 6–26%. The dashed line represents the case assuming a voltage efficiency of 63% and the average capacity factor (11%). The shaded yellow area depicts the impact of the gHB case varying the stack efficiency in the range 60–100% and the capacity factor in the range 6–26%. The dashed yellow line represents the case assuming a stack efficiency of 60% and the average capacity factor (11%).

In terms of economic performance (**Fig. S4**), an increase in voltage efficiency of up to 100% does not create new breakeven points with the bHB and BAU. However, the LCOA at perfect selectivity and ideal voltage efficiency is 74% higher than the value for the BAU for the best location, corresponding to a 34% decrease with respect to the same case for the NH₃-leaf with a 63% voltage efficiency. Moreover, the breakeven point between the gHB and NH₃-leaf shifts to 69% if the ideal voltage efficiency is considered in the best location.

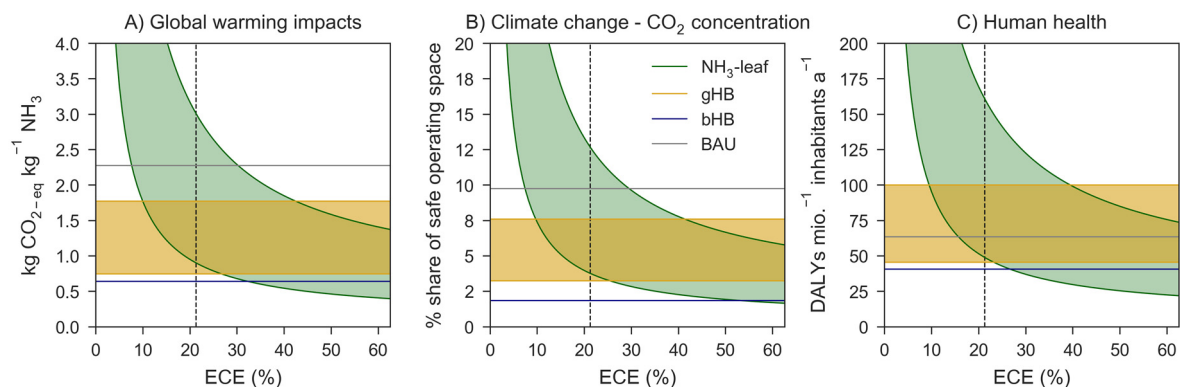


Fig. S5. (A–C) Sensitivities showing the environmental impacts of the ammonia leaf (NH₃-leaf) on three selected metrics (A: global warming impacts; B: climate change – CO₂ concentration; C: human health) versus the energy conversion efficiency (ECE) and comparison with the Haber-Bosch (HB) processes, namely, the green HB (gHB, yellow), blue HB (bHB, blue), and business-as-usual (BAU). In the case of the NH₃-leaf, the voltage efficiency was kept constant at 75%, while the Faradaic efficiency was varied. Regarding the gHB scenario, the stack efficiency was increased from 60 to 70%. The solar capacity factors considered are 6–26%, for both the NH₃-leaf and gHB scenarios.

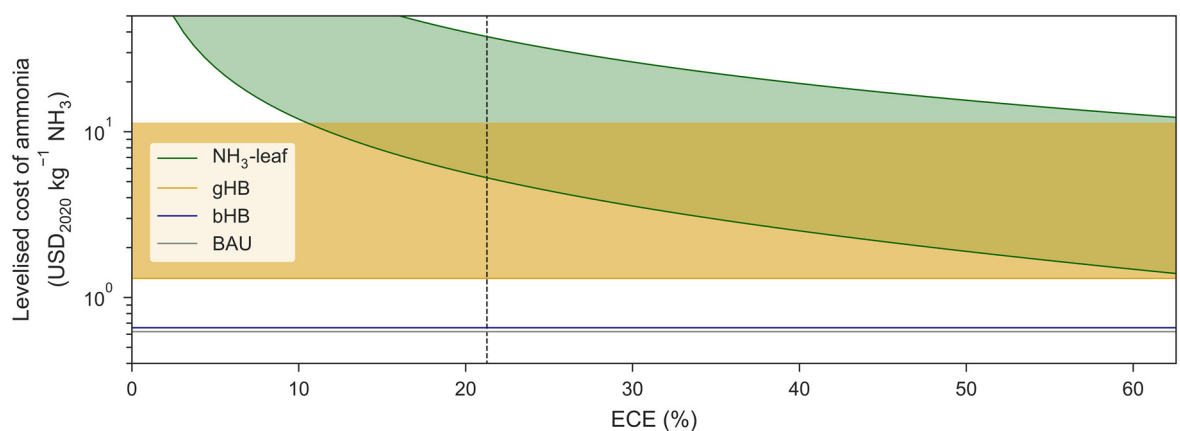


Fig. S6. Economic performance of the ammonia leaf (NH₃-leaf) versus the energy conversion efficiency (ECE) and comparison with the Haber-Bosch (HB) processes, namely, the green HB (gHB, yellow), blue HB (bHB, blue), and business-as-usual (BAU). The NH₃-leaf range spans from a worst-case scenario with 6% solar capacity factor to a best-case scenario with 26% solar capacity factor. The voltage efficiency was kept constant at a value of 75%, while the Faradaic efficiency was varied. Regarding the gHB scenario, the stack efficiency was increased from 60 to 70%.

The consideration of realistically achievable future values for the voltage efficiency of the NH₃-leaf (75%) and the stack efficiency of the water electrolyser of the gHB (70%, against the current value of 60%) does not lead to a qualitatively different behavior than what is highlighted in Fig. S3 (see Fig. S5) in terms of the selected environmental impacts. However, if the economic impacts are instead considered (Fig. S6), the lower bounds of NH₃-leaf and gHB do not show any longer a breakeven point.

In fact, now the NH₃-leaf with 100% Faradaic efficiency displays a value of almost 0.1 USD₂₀₂₀ kg⁻¹ higher than the gHB deployed in the best location. Such finding highlights how the final economic competitiveness and the optimal way in which these technologies will be able to complement each other will be dictated by even mild improvements in the overall energy efficiency of such systems, as well as in transportation costs.

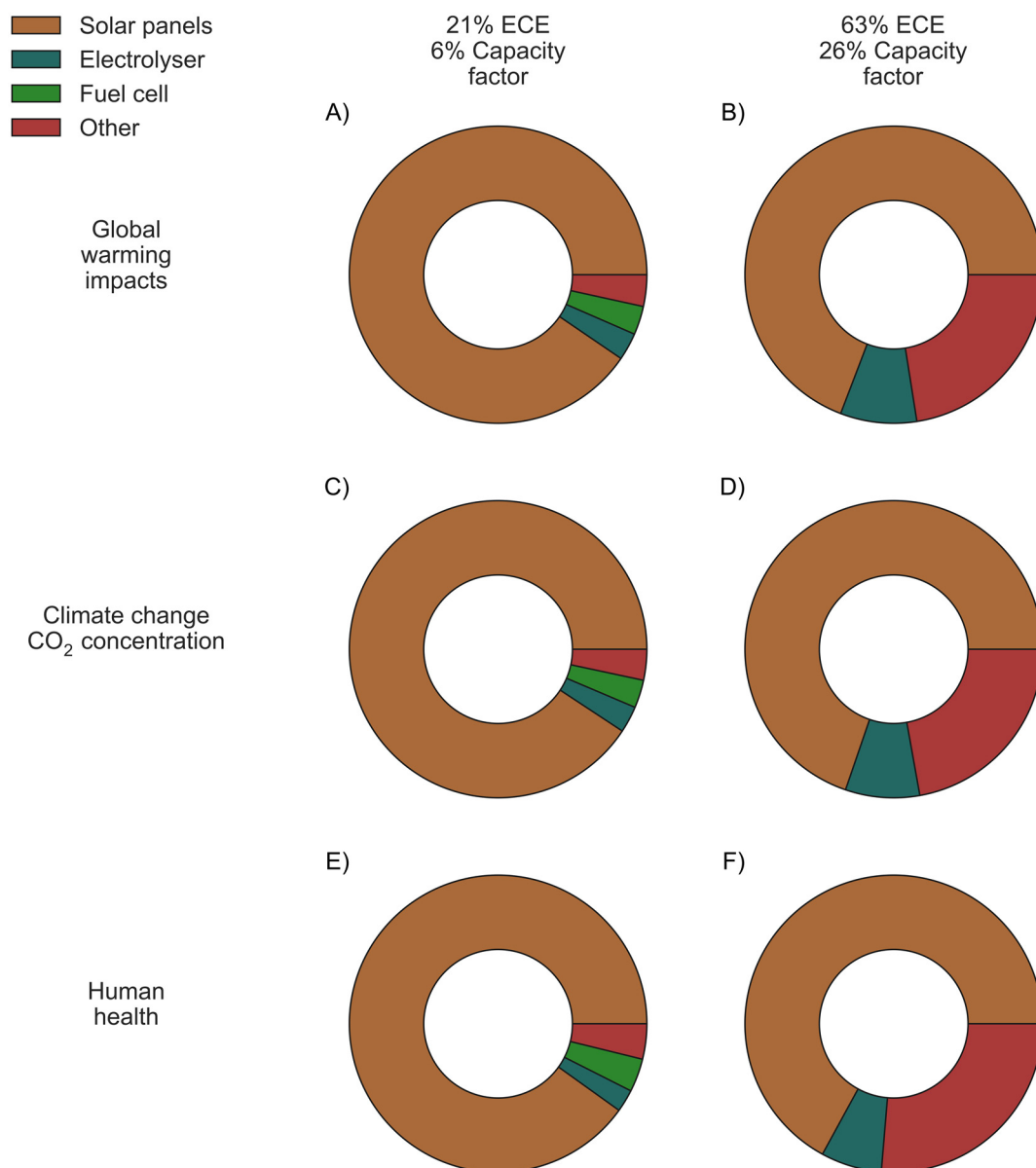


Fig. S7. Breakdown of the impact of the best- and worst-case scenarios with respect to the three key analysed indicators: global warming impacts, impacts on the climate change Earth-system process (considering CO₂ concentration as control variable), and human health damage. In the category “Other”, the water required for reaction and dilution, as well as the electrolyte solution consumption, were both included. For the two scenarios, the capacity factor and the energy conversion efficiency (ECE) were varied.

As expected from the overall behaviour highlighted in **Figs. 2** and **3** of the main manuscript, the impact breakdown shows that the individual system components have the same relative share of the global warming impacts and the impacts on the climate change Earth-system process (**Figs. S7A–S7D**).

The damage to human health also shows a very similar behaviour to the former two indicators in terms of contributions (**Figs. S7E–S7F**). In all the cases, the impact of electricity generation is strongly dominant, with higher values in the worst-case scenarios (**Figs. S7A, S7C, and S7E**), in the range 90-91%, and lower ones in the best cases (**Figs. S7B, S7D, and S7F**), where the contribution drops to 67–70%.

The second most important contribution is associated with the consumption of the electrolyte solution and water (“Other” category), which plays a minor role in the worst scenarios (3–4%) but becomes more relevant in the best cases (22–26%). However, it should be highlighted that this contribution is similar in all the scenarios in absolute values since it is mainly associated with the electrolyte make-up and the final product dilution. In fact, breaking down the category “Other” into its contributors to the global warming impacts, for instance, we find that the water and electrolyte that end up in the final product solution represent from 70% (worst case) to 87% (best case) of the impacts in the “Other” category. Moreover, the electrolyte consumption contributed to the same category of global warming impacts in the range of 69% (best case) to 75% (worst case). The impacts of the electrolyser manufacture play a minor role, representing 2–3% (worst case) up to 7-8% (best case) of the overall impacts. Finally, the fuel cell construction has a low impact in the worst-case scenario (about 3-4%).

Finally, two scenarios were investigated using an NH₃-leaf configuration identical to the one depicted in **Fig. 1** but removing the fuel cell. In the first scenario, the hydrogen by-product was vented, with neither environmental nor economic credits. Conversely, the second scenario assumes that the hydrogen by-product replaces the same amount of hydrogen produced in a PEM water electrolyser. In this case, the associated avoided impact was accounted as a credit and subtracted from the impact of the overall. The assumptions to calculate the credits for the hydrogen by-product at different locations are the same as those described in **Section S.2** for the gHB scenario. **Figs. S8** and **S9** display how the global warming impacts and economic performance of these scenarios vary with the energy conversion efficiency and the assessed range of capacity factors.

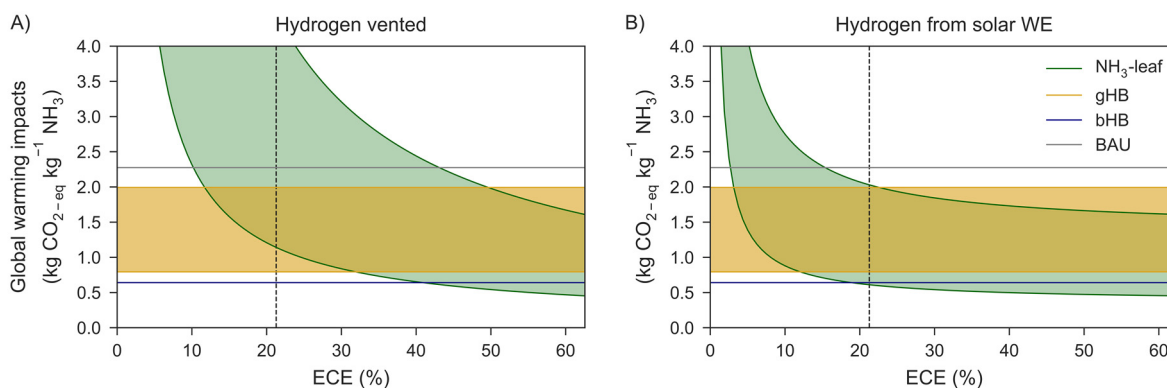


Fig. S8. (A–B) Map showing the global warming impacts of the ammonia leaf (NH_3 -leaf, green) versus the total energy conversion efficiency (ECE), comparing with Haber-Bosch processes, namely, green Haber-Bosch (gHB, yellow), blue Haber-Bosch (bHB, blue), and business-as-usual (BAU, grey). The voltage efficiency was kept constant at 63%, while the Faradaic efficiency was varied. The solar capacity factors considered are 6–26%, for both the NH_3 -leaf and gHB scenarios. (A) Case considering no benefits from the hydrogen by-product, namely, hydrogen venting. (B) Case considering avoided impacts from the substitution of hydrogen produced via PEM water electrolysis.

By examining the environmental impacts of the alternative configuration without fuel cell (**Fig. S8**), different results are achieved depending on the fate of the hydrogen by-product. Specifically, in the case where the hydrogen is vented (**Fig. S8A**), the increased energy consumption leads to higher global warming impacts with respect to the reference scenario with fuel cell. For example, considering state-of-the-art ECE, an increase of the total global warming impacts of *ca.* 7% in the best location is achieved. Consequently, the breakeven efficiencies with respect to the BAU increase, with a value of 10% ECE in the best location. Conversely, when considering the avoided impacts from replacing the hydrogen generated *via* PEM water electrolysis in the same locations (**Fig. S8B**), the system shows improved performance with respect to the reference case with fuel cell. Here, when focusing on the state-of-the-art ECE case deployed in the best location, the global warming impacts decreases by about 43% with respect to the base case. Hence, the breakeven efficiencies decrease drastically, and only 3% ECE is required in the best location to achieve the same environmental performance as the BAU.

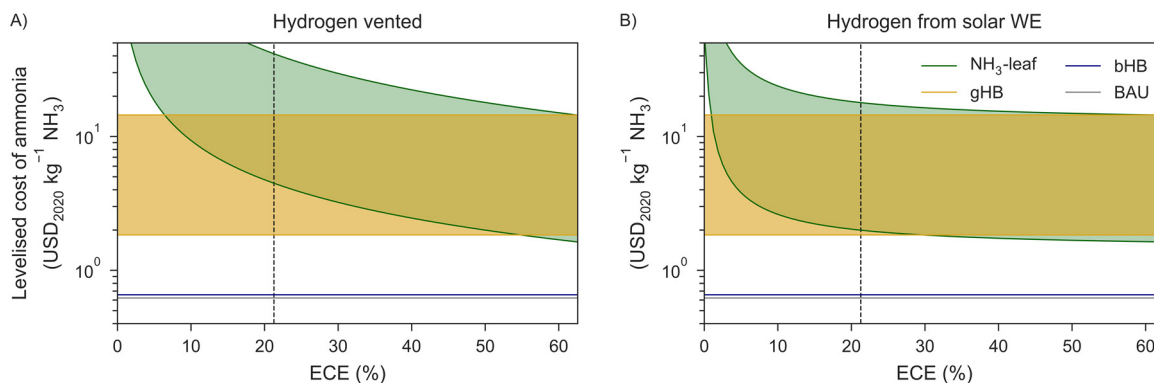


Fig. S9. (A–B) Map showing the the levelised cost of ammonia of the ammonia leaf (NH₃-leaf, green) versus the total energy conversion efficiency (ECE), comparing with Haber-Bosch processes, namely, green Haber-Bosch (gHB, yellow), blue Haber-Bosch (bHB, blue), and business-as-usual (BAU, grey). The voltage efficiency was kept constant at 63%, while the Faradaic efficiency was varied. The solar capacity factors considered are 6–26%, for both the NH₃-leaf and gHB scenarios. (A) Case considering no benefits from the hydrogen by-product, namely, hydrogen venting. (B) Case considering sale of the hydrogen by-product assuming the to use the same production cost obtained from PEM water electrolysis deployed at the same location as the NH₃-leaf.

Concerning the economic performance, the configuration without fuel cell significantly benefits from the avoided fuel cell costs. Because of this, even in the case where hydrogen is not sold (**Fig. S9A**), the overall levelised cost of ammonia decreases. Focusing on the state-of-the-art ECE, a decrease of total economic impact equal to 25% can be achieved at the best location with respect to the case with fuel cell. Such trend is even more evident if the hydrogen by-product is sold at the cost of hydrogen from PEM water electrolysis (**Fig. S9B**). Here, for the same case with the best capacity factor and state-of-the-art ECE, such decrease is equal to about 67%. Similarly, removing the fuel cell leads to lower breakeven efficiencies with respect to the gHB scenario; values of *ca.* 53% and 30% breakeven ECE are attained in the best location for the cases with hydrogen vented and hydrogen sold, respectively.

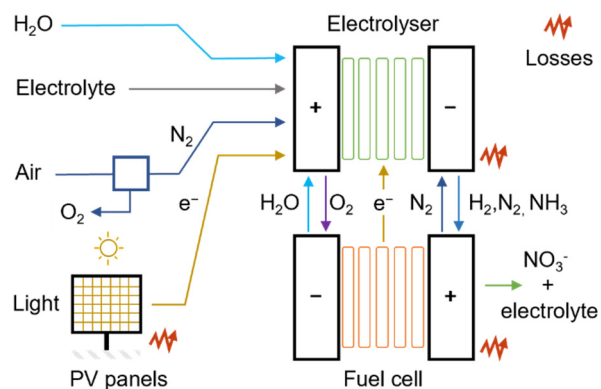


Fig. S10. Schematic representation of a potential NO_3^- -leaf and auxiliary equipment. Water, electrolyte, air, and light are the required inputs. The electrolyser produces diluted ammonia at the cathodic chamber. A fuel cell fed by the produced ammonia, hydrogen and oxygen enables the production of nitrate in the anode and the recycling of electrical energy by valorising undesired hydrogen and oxygen to increase the energy efficiency of the overall system.

References

- 1 G. Towler and R. Sinnott, *Chemical Engineering Design. Principles, practice and economics of plant and process design*, Butterworth-Heinemann, Oxford, 2nd edn., 2013.
- 2 B. M. Comer, P. Fuentes, C. O. Dimkpa, Y. H. Liu, C. A. Fernandez, P. Arora, M. Realff, U. Singh, M. C. Hatzell and A. J. Medford, Prospects and challenges for solar fertilizers, *Joule*, 2019, **3**, 1578–1605.
- 3 S. C. D'Angelo, S. Cobo, V. Tulus, A. Nabera, A. J. Martín, J. Pérez-Ramírez and G. Guillén-Gosálbez, Planetary boundaries analysis of low-carbon ammonia production routes, *ACS Sustain. Chem. Eng.*, 2021, **9**, 9740–9749.
- 4 N. Jungbluth, M. Stucki, K. Flury, R. Frischknecht and S. Büsser, *Life cycle inventories of photovoltaics*, Swiss Centre for Life Cycle Inventories, Uster, 2012.
- 5 L. Bertuccioli, A. Chan, D. Hart, F. Lehner, B. Madden and E. Standen, *Study on development of water electrolysis in the EU*, Fuel Cell and Hydrogen Joint Undertaking, Lausanne, 2014. <https://tinyurl.com/y49hxm7>
- 6 M. Gharibi and A. Askarzadeh, Size and power exchange optimization of a grid-connected diesel generator-photovoltaic-fuel cell hybrid energy system considering reliability, cost and renewability, *Int. J. Hydrogen Energy*, 2019, **44**, 25428–25441.
- 7 M. Fasihi, O. Efimova and C. Breyer, Techno-economic assessment of CO₂ direct air capture plants, *J. Clean. Prod.*, 2019, **224**, 957–980.
- 8 C. Brouwer and M. Heibloem, *Irrigation water management: irrigation water needs*, Food and Agriculture Organisation, Rome, 2013. <https://www.fao.org/3/s2022e/s2022e00.htm>
- 9 P. Heffer, A. Gruère and T. Roberts, *Assessment of fertilizer use by crop at the global level*, International Fertilizer Association and International Plant Nutrition Institute, Paris, 2017. <https://tinyurl.com/mwdc8dhr>
- 10 J. P. Snyder, *Map projections: A working manual*, U.S. Government Printing Office, Washington, DC, 1987. <https://doi.org/10.3133/PP1395>
- 11 S. Pfenninger and I. Staffell, Long-term patterns of European PV output using 30 years of validated hourly reanalysis and satellite data, *Energy*, 2016, **114**, 1251–1265.
- 12 I. Staffell and S. Pfenninger, Using bias-corrected reanalysis to simulate current and future wind power output, *Energy*, 2016, **114**, 1224–1239.
- 13 M. Z. Jacobson and V. Jadhav, World estimates of PV optimal tilt angles and ratios of sunlight incident upon tilted and tracked PV panels relative to horizontal panels, *Sol. Energy*, 2018, **169**, 55–66.
- 14 International Energy Agency, *World Energy Outlook 2019*, OECD Publishing, Paris, 2019.
- 15 H. Althaus, M. Chudacoff, R. Hischier, N. Jungbluth, M. Osses, A. Primas and S. Hellweg, *Life cycle inventories of chemicals.ecoinvent report No.8, v2.0.*, Swiss Centre for Life Cycle Inventories, Dübendorf, 2007.
- 16 S. Evangelisti, C. Tagliaferri, D. J. L. Brett and P. Lettieri, Life cycle assessment of a polymer electrolyte membrane fuel cell system for passenger vehicles, *J. Clean. Prod.*, 2017, **142**, 4339–4355.
- 17 M. B. Freilich and R. L. Petersen, in *Kirk-Othmer Encyclopedia of Chemical Technology*, John Wiley & Sons, Ltd., New York, NY, 2000.
- 18 R. D. Johnson, *NIST computational chemistry comparison and benchmark database*, National Institute of Standards and Technology, Gaithersburg, 2011. <https://doi.org/10.18434/T4D303>
- 19 G. Lauer mann, P. Häussinger, R. Lohmüller and A. M. Watson, in *Ullmann's Encyclopedia of Industrial Chemistry*, Wiley-VCH Verlag GmbH & Co. KGaA, Weinheim, Germany, 2013, pp. 1-15.

- 20 X. Liu, A. Elgowainy and M. Wang, Life cycle energy use and greenhouse gas emissions of ammonia production from renewable resources and industrial by-products, *Green Chem.*, 2020, **22**, 5751–5761.
- 21 G. Peng, J. Wu, M. Wang, J. Niklas, H. Zhou and C. Liu, Nitrogen-defective polymeric carbon nitride nanolayer enabled efficient electrocatalytic nitrogen reduction with high Faradaic efficiency, *Nano Lett.*, 2020, **20**, 2879–2885.
- 22 A. Valente, D. Iribarren, J. Dufour and G. Spazzafumo, Life-cycle performance of hydrogen as an energy management solution in hydropower plants: A case study in Central Italy, *Int. J. Hydrogen Energy*, 2015, **40**, 16660–16672.
- 23 HyLYZER[®]-200 HyLYZER[®]-250,
<https://mart.cummins.com/imagelibrary/data/assetfiles/0070332.pdf> (accessed 30 March 2022).
- 24 D. A. Notter, K. Kouravelou, T. Karachalios, M. K. Daletou and N. T. Haberland, Life cycle assessment of PEM FC applications: electric mobility and μ -CHP, *Energy Environ. Sci.*, 2015, **8**, 1969–1985.
- 25 B. Parkinson, P. Balcombe, J. F. Speirs, A. D. Hawkes and K. Hellgardt, Levelized cost of CO₂ mitigation from hydrogen production routes, *Energy Environ. Sci.*, 2019, **12**, 19–40.
- 26 M. Yang and K. A. Rosentrater, Techno-economic analysis of the production process of structural bio-adhesive derived from glycerol, *J. Clean. Prod.*, 2019, **228**, 388–398.
- 27 IRENA, *Renewable Power Generation Costs in 2018*, International Renewable Energy Agency, Abu Dhabi, 2019.
<https://tinyurl.com/2fn8ackv>